NIH Public Access
Author Manuscript
J Opt Soc Am A Opt Image Sci Vis. Author manuscript; available in PMC 2008 November 5.

Published in final edited form as:
J Opt Soc Am A Opt Image Sci Vis. 2007 May ; 24(5): 1457–1467.

Reduced-illuminance autofluorescence imaging in *ABCA4*-associated retinal degenerations

Artur V. Cideciyan, **Malgorzata Swider**, **Tomas S. Aleman**, **Marisa I. Roman**, **Alexander Sumaroka**, and **Sharon B. Schwartz**
Scheie Eye Institute, Department of Ophthalmology, University of Pennsylvania, Philadelphia, Pennsylvania 19104, USA

Edwin M. Stone
Howard Hughes Medical Institute and Department of Ophthalmology, University of Iowa Hospitals and Clinics, Iowa City, Iowa 52242, USA

Samuel G. Jacobson
Scheie Eye Institute, Department of Ophthalmology, University of Pennsylvania, Philadelphia, Pennsylvania 19104, USA

Abstract

The health of the retinal pigment epithelium (RPE) can be estimated with autofluorescence (AF) imaging of lipofuscin, which accumulates as a byproduct of retinal exposure to light. Lipofuscin may be toxic to the RPE, and its toxicity may be enhanced by short-wavelength (SW) illumination. The high-intensity and SW excitation light used in conventional AF imaging could, at least in principle, increase the rate of lipofuscin accumulation and/or increase its toxicity. We considered two reduced-illuminance AF imaging (RAFI) methods as alternatives to conventional AF imaging. RAFI methods use either near-infrared (NIR) light or reduced-radiance SW illumination for excitation of fluorophores. We quantified the distribution of RAFI signals in relation to retinal structure and function in patients with the prototypical lipofuscin accumulation disease caused by mutations in *ABCA4*. There was evidence for two subclinical stages of macular *ABCA4* disease involving hyperautofluorescence of both SW- and NIR-RAFI with and without associated loss of visual function. Use of RAFI methods and microperimetry in future clinical trials involving lipofuscinopathies should allow quantification of subclinical disease expression and progression without subjecting the diseased retina/RPE to undue light exposure.

1. INTRODUCTION

Lipofuscin refers to granules made of heterogeneous molecules that accumulate in the retinal pigment epithelium (RPE) as a result of photoreceptor outer segment (OS) phagocytosis.[1] Lipofuscin contains several distinct fluorophores,[2] which include A2E.[3] Understanding of the biogenesis of A2E accumulation in the RPE has been dramatically advanced in recent years.[4] It is currently hypothesized that the photoisomerized chromophore all-*trans*-retinal in rod photoreceptor cells forms an adduct with phosphatidylethanolamine on the inner leaflet of rod OS membranes. The ABCA4 protein located at photoreceptor OS rims is involved in flipping this adduct from the inner to outer leaflet, where it is reduced to all-*trans*-retinol. Under certain light regimes a proportion of the adduct is trapped within the OS and, upon phagocytosis of the OS ends, the trapped material is transformed to A2E in RPE. Consistent with this

Correspondence to: Artur V. Cideciyan.
Corresponding author Artur V. Cideciyan can be reached by e-mail at cideciya@mail.med.upenn.edu..

NIH-PA Author Manuscript
NIH-PA Author Manuscript
NIH-PA Author Manuscript

NIH-PA Author Manuscript

NIH-PA Author Manuscript

NIH-PA Author Manuscript

hypothesis, abnormal ABCA4 function and exposure to light causes dramatic increase in A2E accumulation in mice.[5,6] Many lines of evidence suggest that abnormal A2E/lipofuscin accumulation may be toxic to the RPE[4,7] and results in degeneration of the retina and vision loss owing to what may be termed a "lipofuscinopathy." Pharmaceutical treatment strategies based on inhibition of the visual cycle or reduction of vitamin A supply to the eyes have been proposed to slow the natural history of lipofuscinopathies such as Stargardt disease (STGD) and age-related macular degeneration (AMD).[6,8-11]

Over the past decade, autofluorescence (AF) imaging has become a convenient method for determining the distribution of lipofuscin noninvasively in human subjects (see, e.g., Refs. [12-28]). The method is ideal for quantitatively delineating regions of abnormal lipofuscin accumulation as well as RPE disease and atrophy. AF imaging is thought to be appropriate for natural history studies and as outcome measures of therapeutic interventions in *ABCA*4-associated retinal degenerations and AMD.[29] Conventional AF imaging is performed with short-wavelength (SW) high-intensity excitation light which, and at least in principle, could contribute to the A2E accumulation and/or photooxidation and thus confound the underlying natural history of disease. This may be especially relevant in a clinical trial setting where imaging is performed repeatedly at regular intervals. The same argument applies to fluorescein angiography and fundus photography.[30]

In the current work, we considered reduced-illuminance alternatives to conventional AF imaging such that a quantitative estimate of the primary disease feature can be obtained in lipofuscinopathies with less risk of modifying the natural history of lipofuscin accumulation. Reduced *illuminance* can be achieved either by reducing the retinal irradiance and/or exposure duration of excitation wavelengths absorbed by photoreceptors and lipofuscin, or by choosing excitation wavelengths significantly displaced from photoreceptor and lipofuscin absorption maxima. Accordingly, reduced-illuminance AF imaging (RAFI) was performed with SW and near-infrared (NIR) light.[31-33] NIR-reflectance imaging was used in place of fundus photography. Microperimetry and optical coherence tomography (OCT) were also used to extend the information content available for interpretation of the results.

2. METHODS

A. Subjects

Subjects (n=8, ages 22-47) with normal retinas and patients (n=7, ages 21-53) with macular degeneration were included in the study. Six of seven patients had the diagnosis of STGD and known or suspected disease-causing *ABCA*4 mutations; patient 7 had bilateral maculopathy of uncertain etiology (Table 1). Research procedures were in accordance with institutional guidelines and the Declaration of Helsinki. All patients gave written informed consent.

B. *En Face* Imaging with Scanning Laser Ophthalmoscope

A second-generation confocal scanning laser ophthalmo-scope (cSLO), HRA2 (Heidelberg Engineering, Dossenheim, Germany) was used to perform *en face* imaging. Much of the methodology was similar to our previous studies with HRA1.[34,35] All HRA2 imaging was performed with the high-resolution mode, where a 30° × 30° region of the retina is sampled onto a 1536 × 1536 pixel image and consecutive frames can be obtained at the rate of 4.7 Hz. HRA2 uses three solid-state lasers[25] with maxima at 488, 790, and 820 nm. For SW-RAFI, 488 nm excitation was used after reducing the power output (at the cornea) from the manufacturer's setting of ~ 300 to ~ 95 μW. We estimate[36] this lower corneal power to result in an equivalent retinal irradiance of ~ 100 μW cm^{-2}. Retinal exposure was limited to less than 60 s per retinal region imaged, resulting in a worst-case retinal dose of <6 mJ cm^{-2}. For reference, the most light-sensitive large vertebrate eye known to date (rhodopsin mutant

NIH-PA Author Manuscript

NIH-PA Author Manuscript

NIH-PA Author Manuscript

dog[36]) has a white-light damage threshold between 6 and 60 mJ cm^{-2} in the pigmented RPE region of the eye; the tapetal (nonpigmented) retinal region of these dogs shows even greater sensitivity to light,[36] with light damage thresholds below 6 mJ cm^{-2}.

For NIR-RAFI, 790 nm excitation was used at a corneal power of 2.5 mW, unchanged from the manufacturer's setting. For NIR-reflectance imaging, 820 nm light was used after reducing the power output (at the cornea) from the manufacturer's setting of 100 to 15 μW. Lower power allowed visualization of fundus structures in diseased retinas that otherwise tend to saturate the detector owing to higher-than-normal reflectance presumed to be due to depigmentation of the RPE. Internal blue (peak 460 nm) LED fixation lights were used.

Both SW- and NIR-RAFI were performed with an HRA2 sensitivity setting of 95%. The resulting images appear dark (~ 40 gray-scale units) and noisy on the acquisition screen; for reference, conventional AF imaging with the same HRA2 instrument using the higher-illumination intensity and 88% sensitivity setting produces images of average intensity similar to those of SW-RAFI with the 95% setting. Use of the same detector sensitivity setting for SW- and NIR-RAFI has the additional advantage of providing images with comparable black levels. Laser power levels were checked monthly for calibration drift. Detector gain and offset corresponding to the 95% sensitivity setting were regularly checked and recorded with the use of the service module of the software, and overall system throughput was confirmed by imaging solid fluorescence standards.

The fully dilated pupil of the subject was aligned with the optical axis of the instrument (head position stabilized with chin and forehead rests) in a room with dimmed lights. The focus setting was optimized, and NIR-reflectance images were acquired at nine overlapping "standard" regions corresponding to the nine internal fixation light choices of the HRA2. A 10th field nasal to the optic nerve was imaged without fixation. Next, NIR-RAFI imaging was performed at the same 10 locations. The focus setting was optimized to produce the brightest image. At each retinal location, a "stack" of 25 consecutive images was obtained. Next, room lights were turned on and SW-RAFI imaging was performed after optimizing the focus setting. At each retinal location, a "stack" of 25 consecutive images was obtained; total illumination time at each retinal region did not exceed 60 s and was typically 10-15 s.

C. Processing of Confocal Scanning Laser Ophthalmoscope Images

HRA2 image frames or image stacks were exported using the "BMP Export" facility of the manufacturer's software, and all further processing was performed either with IMAGEJ (version 1.37c; http://rsb.info.nih.gov/ij; developed by Wayne Rasband and provided in the public domain by the National Institutes of Health, Bethesda, Maryland) or with custom written programs in MATLAB (The Math-works, Natick, Massachusetts). Image stacks were visually examined, and frames with blinks and midframe eye movements were discarded. In some cases, a filter was used to deinterlace (replace odd lines with the average of even lines) images in which alternating lines appeared shifted owing to low signal-to-noise ratio. Resolution was reduced from 1536 × 1536 to 512 × 512 by averaging 3 × 3 blocks of pixels. Ten frames from each stack were chosen and then automatically registered using a pair of programs (TURBOREG and STACKREG; http://bigwww.epfl.ch/algorithms.html/; provided in the public domain by the Bioengineering Group; Ecole Polytechnique Federale de Lausanne, Switzerland), and the mean intensity was calculated. Mosaicing was performed by manually specifying retinal landmark pairs corresponding to pairs of frames showing overlapped retinal regions.

Previous studies in patients with retinal degenerative diseases have shown that the local heterogeneity of the AF intensity correlates with local disease severity.[24,34,35] In the current work, we used a run-length-based[37] measure of local AF intensity heterogeneity to quantify

NIH-PA Author Manuscript

NIH-PA Author Manuscript

NIH-PA Author Manuscript

SW-and NIR-RAFI; the method used was slightly modified from our previous description.[35] In brief, a primitive called a gray-level run, is defined as the set of consecutive, collinear pixels in a predefined direction having a criterion similarity of gray level; for the current work, similarity was defined as having an intensity within 10%. Run length is the number of pixels belonging to a gray-level run such that image regions with heterogeneous intensity have a shorter run length compared with regions with more homogeneous intensity.[38] To quantify the local AF intensity heterogeneity, we calculated the mean run length at each pixel along the eight principle directions after spatially filtering the SW- or NIR-RAFI intensity with a Gaussian filter (radius 5 pixels) to minimize the contribution of the noise produced by the avalanche photodiode detector. A direction was not included in the average if a pixel corresponding to the edge of the frame was contained with the gray-level run. The result of this texture analysis method is a calculated image where the value of each pixel represents the mean radius of a circular region over which the AF intensity would be expected to be nearly homogeneous. Another Gaussian filter (radius 5 pixels) was applied to the resulting run-length image.

D. Imaging with Optical Coherence Tomography

In vivo microstructure of the retina was quantified with OCT3 (Zeiss Humphrey Instruments, Dublin, California) and protocols previously described.[34,39,40] In patients with central vision loss, the anatomical fovea was determined by moving the scan location with respect to the fixation location until the telltale signs of a foveal depression were visualized. Overlapping linear scans of 4.5 mm length were acquired along the horizontal meridian extending 30° from the anatomical fovea. At least three OCT images were obtained at each retinal location. A video fundus image was acquired and saved with each OCT scan by the commercial software. In addition, the fundus video visible during the complete session was recorded continuously on a video cassette recorder.

E. Processing of Optical Coherence Tomography Data

Postacquisition processing of OCT data was performed with custom programs (MATLAB 6.5, MathWorks, Natick, Massachusetts). Longitudinal reflectivity profiles (LRPs) making up the OCT scans were aligned using a dynamic cross-correlation algorithm[41] with a manual override when crossing structures (for example, intraretinal pigment), which interrupted local lateral isotropy of signals. At times, repeated scans were averaged to increase the signal-to-noise ratio and allow better definition of retinal laminae.[36,39]

Retinal thickness was defined as the distance between the signal transition at the vitreo-retinal interface and the major signal peak corresponding to the RPE.[40] In normal subjects, the RPE peak was assumed to be the last peak within the 2- or 3-peaked scattering signal complex deep in the retina. In patients, the presumed RPE peak was sometimes the only signal peak deep in the retina; other times, it was apposed by other major peaks. In the latter case, the RPE peak was specified manually by considering the properties of the backscattering signal originating from layers vitread and sclerad to it.

Wide-field OCT scans were produced by mosaicing overlapping shorter OCT scans. The lateral extent of the OCT scans was calibrated against HRA2 images by registering a central OCT video image for each subject with an appropriate HRA2 image. The scale factor, when non-unity, was used to scale the lateral dimension of the OCT scans.

Using OCT scans, the axial extent of propagation of the NIR light was estimated from the normalized partial integral of the backscattering signal over retinal depth from the RPE signal peak toward the scleral direction.[40] The partial integral was divided by the signal intensity at the RPE peak in order to normalize for the pre-RPE attenuation of the light intensity. We refer

NIH-PA Author Manuscript

NIH-PA Author Manuscript

NIH-PA Author Manuscript

to the resulting measure as sub-RPE backscattering index (sRBI). Under the simplifying assumption of dominant backscattering and absorption of the NIR light occurring at or near the normal RPE, sRBI may be expected to be proportional to the amount of NIR light reaching the choroidal layers. This expectation is consistent with experimental results in animals with varying RPE and choroidal pigmentation[41] and in patients with molecularly defined choroideremia and depigmentation of the RPE.[40]

F. Microperimetry

Visual function testing was performed with a microperimeter (MP1, Nidek Technologies America Inc, Greensboro, North Carolina). MP1 uses NIR light to image the retina and track retinal landmarks specified at the start of the test. Tracking is performed in real time, and stimulus locations are adjusted according to the real-time gaze information to be presented on a prespecified test pattern defined on the retina. In all subjects, we used a "foveo-papillary profile" as our custom designed test pattern, which consisted of stimulus locations extending along the horizontal meridian starting at 0.5° nasal to the anatomical fovea and extending to 16° nasal retina on a 0.5° grid. Testing was performed in fully dark-adapted subjects with a dim red mesopic background and Goldmann III-sized (200 ms duration) stimuli. Both red and white stimuli were used to extend the effective dynamic range of this instrument from 2 log units (for each stimulus individually) to ~ 3 log units (using thresholds from both stimuli); the mesopic effectiveness of the two stimuli overlap by ~ 1 log unit. The lateral extent of the MP1 profiles were calibrated against HRA2 images, and scale factors were applied to bring them into registration.

3. RESULTS

A. Normal RAFI

The NIR-reflectance image in a representative normal subject [Fig. 1(a), same subject as that shown in Fig. 1A of Ref. 35] shows a spatially homogeneous appearing macular region surrounded by increasing heterogeneity. Some of this perimacular heterogeneity is due to the visibility of choroidal features.[42] SW-RAFI in the same subject [Fig. 1(b)] has familiar features expected from conventional AF imaging (e.g., Refs. 12-28). There is a small (~ 2° diameter) dark region at the fovea dominated by absorption of the SW illumination by macular pigment.[43] An annular region (extending to ~ 5° from the fovea) of relatively low AF intensity surrounds the dark center. Highest AF intensities correspond to retinal regions 10-15° eccentric from the fovea.[19] Darker blood vessels are contrasted against a brighter background, and there is a dark optic nerve head.

NIR-RAFI in the same normal subject [Fig. 1(c)] shows similarities and differences as compared with NIR reflectance and SW-RAFI. There is a broad (~ 10° diameter) region of higher intensity on NIR-RAFI near the fovea,[33] as opposed to the lower intensity seen in SW-RAFI; there is no major local contrast in NIR reflectance in this region. A subset of normal subjects shows a small (~ 1° diameter) region of low intensity apparent at the fovea both in NIR-RAFI and in NIR reflectance (data not shown). NIR-RAFI in the macular region appears more uniform than in the perimacular region where choroidal structures are visible; this is similar to NIR-reflectance images [Fig. 1(c)]. The optic nerve head has lower intensity than in NIR-RAFI, similar to SW-RAFI but dissimilar to NIR reflectance. The boundary between the optic nerve head and the retinal background appears much sharper in NIR-RAFI compared with the gradient apparent on SW-RAFI;[35] a greater loss of SW excitation light through the thicker nerve fiber layer[44] could contribute to this effect.

Quantitative features of these reduced illuminance modalities can be appreciated along horizontal profiles [Fig. 1(d)] and be correlated with the retinal cross section by OCT, which

NIH-PA Author Manuscript

NIH-PA Author Manuscript

NIH-PA Author Manuscript

is based on backscattering and absorption differences among retinal laminae under NIR light [Fig. 1(e)]. The highest-intensity central region on NIR-RAFI corresponds to the central region of least backscatter originating from sub-RPE layers on OCT [Fig. 1(e), single line]. Similarly, the temporal region of NIR-RAFI that shows the appearance of choroidal vasculature [Fig. 1 (c)] corresponds to the OCT region of the greater sub-RPE backscatter signal [Fig. 1(e), double line].

B. RAFI in Localized Abnormalities of Photoreceptors and Retinal Pigment Epithelium

Distinct boundaries between retinal disease and health can help evaluate alternative hypotheses about tissue origins of imaging signals.[40] The left eye of patient 7 presents such an opportunity. On NIR-reflectance imaging [Fig. 2(a)] there is a central lesion of ~ 12° diameter with sharp boundaries; a thin vertical peninsula of healthier retina extends downward from the superior lesion boundary and ends near the preserved fovea (with 20/25 visual acuity). Visibility of choroidal blood vessels within the central lesion suggests loss of normal RPE pigmentation. On SW-RAFI the lesion appears dark, corresponding to loss of lipofuscin secondary to diseased and/or atrophic RPE [Fig. 2(b)]. There is an irregular annulus of high autofluorescence surrounding the lesion [Fig. 2(b)]. NIR-RAFI shows a pattern generally similar to SW-RAFI with a lower intensity central lesion and a surrounding annulus of high intensity [Fig. 2(c)]. Within the central lesion, darker choroidal vessels appear to be blocking a diffuse and low-intensity NIR-RAFI signal originating from deeper layers [Fig. 2(c)]. An OCT scan across the lesion [Fig. 2(c), inset] shows thinning of the parafoveal retina and a dramatic increase in backscatter originating from layers deep to the RPE [Fig. 2(c), inset, triple white lines]. In normal OCT, backscatter from choroidal layers is much less detectable owing to presumed absorption and/or scattering of this wavelength at/near the RPE- choriocapillaris region [Fig. 1(e)]. The results in the normal subjects (Fig. 1) and in the patient with maculopathy (Fig. 2) confirm the previously proposed hypothesis that fluorophores in the RPE and choroid can be activated by NIR excitation.[33] Our results extend previous work by detecting retinal locations suspect for increased choroidal contribution to NIR-RAFI with the use of an OCT-derived measure of sub-RPE backscattering amplitude as a local index of the depth of penetration of the NIR light.

C. Macular *ABCA4* Disease Sequence: Correlation of RAFI with Visual Function and Retinal Structure

Human lipofuscinopathies caused by *ABCA4* mutations can show dramatic variation in spatial distribution and severity of retinal disease.[34,35,45-50] Our previous work suggested that the region between the fovea and the optic nerve may be informative of the entire gamut of *ABCA4* disease expression and that tests of structure and function densely sampling this region may form sensitive measures of natural history or outcome of therapy.[35] In the current work, we used RAFI, microperimetry, and OCT to sample this region.

Patient 6 illustrates mild/early *ABCA4* disease of the macula (Fig. 3). NIR-reflectance imaging, SW-, and NIR-RAFI show a central region of abnormality extending to ~ 5° eccentricity [Figs. 3(a), 3(c), and 3(d)]. Within this region there is a small (~ 2° diameter) area of increased reflectance [Fig. 3(a)] and reduced fluorescence [Figs. 3(c) and 3(d)] visible immediately nasal to the fovea. This area likely corresponds to severe RPE disease or atrophy, and a colocalized scotoma on microperimetry [Fig. 3(b)] and increased backscatter on OCT [Fig. 3(e)] are consistent with this interpretation. Foveal sparing is visible as an island of relative homogeneity of fluorescence, whereas the parafoveal region shows spatial heterogeneity. The retinal region surrounding the central ~ 10° diameter maculopathy appears qualitatively normal.

Visual function, retinal structure, and RAFI were studied quantitatively along horizontal foveo-papillary profiles with special emphasis on the perifoveal retinal region with normal

NIH-PA Author Manuscript

NIH-PA Author Manuscript

NIH-PA Author Manuscript

appearance. The only area showing normal parameters in all measures was about 1.5° wide and located between 10.5° and 12° eccentric from the fovea immediately temporal to the optic nerve. Based on previous work[34] we defined this as stage I disease. A neighboring ~ 4° wide area between 6.5° and 10.5° eccentric from the fovea showed supernormal intensity with SW- and NIR-RAFI [Figs. 3(c) and 3(d), insets]; all other parameters were within normal limits. The next definable area was ~ 2° wide between 4.5° and 6.5° eccentric where visual function measured by microperimetry became abnormal. These two subclinical stages were defined as stages IIa and IIb, respectively, based on the subclinical stage II disease previously defined.[34] Closer to the fovea there were increasing abnormalities in different modalities. Between ~ 2.5° and 4.5° eccentric, there were losses of visual sensitivity, supernormal SW- and NIR-RAFI intensities, and variable abnormalities in local homogeneity of autofluorescence. Between ~ 0.5° and 2.5° eccentric, there was severe loss of visual sensitivity, counterintuitive return of SW-RAFI to *normal*, and indeterminable NIR-RAFI associated with dramatic increase in backscatter intensity originating from sub-RPE layers [Fig. 3(e), inset]. At the fovea, NIR-RAFI was normal, whereas SWRAFI was dramatically supernormal, consistent with the loss of macular pigment optical density in *ABCA*4 disease.[51]

A summary of the quantitative multiparameter analysis in the foveo-papillary region of six patients is shown in Fig. 4. Areas of subclinical stage II disease were always sandwiched between the clinically overt maculopathy and the optic nerve or the area of stage I disease. Stage IIa disease (hyperautofluorescence with normal function) was always more eccentric to stage IIb disease (hyperautofluorescence with visual dysfunction). The transition from stage II to more severe disease corresponded to an increase in spatial heterogeneity of autofluorescence. In some cases there was evidence for the abnormal heterogeneity boundary in NIR-RAFI to be more peripheral than that in SW-RAFI (P1, P2, P6) or vice versa (P3, P4, P5), but in most cases, peripheral boundaries of the onset of these abnormalities were within about 1° of one another. Parafoveal regions of abnormally increased sRBI could correspond to normal (P2, P5, P6) or hyperautofluorescence (P1, P3, P4) on SW-RAFI, suggesting the existence of diseased RPE (as opposed to RPE atrophy) in these early/mild disease stages. Indeed, none of the patients studied had abnormally reduced autofluorescence in the foveo-papillary region analyzed. In two of the patients with the largest extents of maculopathies (P2 and P4), there were perifoveal regions of abnormally *reduced* sRBI on OCT. In five of six patients, there was foveal hyperautofluorescence with SW-RAFI but normal fluorescence with NIR-RAFI; P4 showed hyperautofluorescence with both SW and NIR modalities. Interpretation of the foveal findings will have to take into account not only RPE abnormalities[33] but also consequences of retinal abnormalities[51] and differences in choroidal pigmentation.[33]

4. DISCUSSION

Molecular understanding of the biogenesis and toxicity of lipofuscin over the past two decades[1-7] has led to potential treatment strategies designed to slow its accumulation in human diseases such as STGD and AMD.[6,8-11] Outcome of therapeutic strategies can be objectively measured with AF imaging—the only direct measure of lipofuscin accumulation.[29] Conventional AF imaging has been applied to various patient populations for more than a decade,[12-28,34,35] and recently there has been a call for standardization and quantification.[52] It is an unfortunate coincidence that the high-intensity SW illumination used for conventional AF imaging of lipofuscin is also a risk factor contributing to the accumulation and toxicity of the same substance. Of course, all ophthalmic imaging instruments, including those used for AF imaging, are designed to operate safely below retinal light damage thresholds, and there have been no reports of acute light damage due to AF imaging. Yet it is important to keep in mind that damage thresholds are based mostly on normal retinas, whereas ophthalmic imaging is performed mostly in diseased retinas,[53] and there is increasing evidence

NIH-PA Author Manuscript

NIH-PA Author Manuscript

NIH-PA Author Manuscript

that some retinal degenerative diseases have lower light damage thresholds.[36,54] Therefore it would be prudent to reduce as much as is technically possible the light exposure used in patients with retinal degenerative conditions until the extent of disease-associated photosensitivity of the human retina is better understood. This is especially true for shorter wavelength "actinic" lights and under conditions of repetitive examination, such as in a clinical trial. The current work attempted to take a step in this direction with the quantitative use of RAFI methods.

SW-RAFI was designed to be a lower light-dose replacement for conventional AF imaging. The lower illumination was also more comfortable for the subjects to view. Shortcomings of SW-RAFI included noisier and darker images apparent on the acquisition screen, making the imaging task more difficult for the operator. Another disadvantage was the necessity to use additional image processing steps not included in the manufacturer's software. With postacquisition processing however, SW-RAFI results were both qualitatively and quantitatively comparable to those in the rapidly growing literature on conventional AF imaging (e.g., Refs. 12-28, 34, and 35). Specifically, observation of hyperautofluorescent regions with spatial homogeneity in early *ABCA*4 disease and spatially heterogeneous regions in later disease stages were consistent with previous work using quantitative conventional AF imaging.[34,35] Optimization of the appearance of images on the acquisition screen by the manufacturer may allow even further reduction in SW illuminance in the future.

AF imaging with NIR excitation, NIR-RAFI, is inherently low luminance owing to separation of this wavelength from the region of photoreceptor pigment absorption. Indeed NIR-RAFI illumination is nearly imperceptible for most patients (it appears as a dim red light to normal eyes). NIR excitation light is also separated from the SW region of lipofuscin photoreactivity.[7] NIR-RAFI is a new modality,[31-33] however, and the interpretation of the images is not well established. One of the leading hypotheses[33] proposes that melanin (or related) fluorophores in the RPE and in the choroid contribute variably to the NIR-RAFI signal, and our data are consistent with this hypothesis. Our use of colocalized OCT scans showed a correspondence between retinal locations of abnormally increased choroidal penetration of NIR light and significantly increased choroidal component to the NIR-RAFI signal; these regions of choroidal signal enrichment were excluded from quantitative analyses in the current work. There were also some disease stages in which apparent RPE or sub-RPE deposits abnormally reduced choroidal penetration of NIR light. At such retinal locations, NIR-RAFI would be expected to be enriched with signals from RPE fluorophores. Future experimental studies seeking to define the absorption and scattering properties of the RPE, lipofuscin, and sub-RPE deposits under NIR light may allow quantitative use of NIR penetration estimates from OCT to distinguish between RPE and sub-RPE components of the NIR-RAFI.

Perifoveal hyperautofluorescence with SW-RAFI without associated overt disease may have been a predictable subclinical disease stage in patients with *ABCA*4 mutations.[5,16,21,22,24,34,35] Yet the finding of colocalized hyperautofluorescence with both SW- and NIR-RAFI modalities was unexpected. Assuming the dominant fluorophore of the NIR-RAFI is melanin, melanolipofuscin, or a related pigment, there are at least three hypotheses to consider. First, newly synthesized melanin could be deposited in the diseased RPE together with increased lipofuscin accumulation. Although it is thought that adult mammalian RPE cells lack melanogenesis, there has been some evidence consistent with slow melanin production in the RPE throughout life.[55] Second, the optical cross section of existing melanin granules in the RPE could be increased by apical displacement[1,56] due to abnormal lipofuscin accumulation or by active transport.[57] Such increase in melanin optical cross section would be expected to decrease SW excitation light reaching more distal lipofuscin granules and thus cause SW-RAFI to grossly underestimate the lipofuscin accumulation. Third, increased RPE stress in *ABCA*4 disease could change the properties of melanin granules. Consistent with this hypothesis is the finding of dramatically increased autofluorescence emanating from oxidized melanin.[58]

NIH-PA Author Manuscript

NIH-PA Author Manuscript

NIH-PA Author Manuscript

Alternative hypotheses involving fluorophores different from melanin co-accumulating with RPE lipofuscin cannot be ruled out at this time. Many of these hypotheses can be directly tested in animal models of lipofuscin accumulation.[5,6]

We have previously defined disease stages in the midperipheral retina of human patients with retinopathy due to *ABCA*4 mutations,[34] but very little was known about equivalent stages in the macular region. Current work showed the existence of two subclinical disease stages in the perifoveal region. The earliest detectable disease (stage IIa) was hyperautofluorescence with normal retinal function and structure, and this was similar to the earliest disease stage observed in the midperiphery. The next macular disease stage (stage IIb) was hyperautofluorescence *and* abnormal visual function, and this was different from midperipheral retina where loss of visual function occurs in late disease.[34] Our results allow the speculation that macular retina may react differently from peripheral retina to the accumulation of lipofuscin. Alternatively, there could be *retinal* fluorophores causing visual dysfunction and contributing to the AF signal.[59-61] One such moiety has been hypothesized to be A2-rhodopsin.[62] Future AF studies in experimental animals may be required to better understand all the contributors to SW- and NIR-RAFI signals in health and disease. In the meantime, RAFI should remain an important tool for estimating the natural history of disease progression and the outcome of therapies in lipofuscinopathies.

ACKNOWLEDGMENTS

This research is supported by National Institutes of Health grant EY-013203, Macula Vision Research Foundation, Foundation Fighting Blindness, Macular Disease Foundation, Ruth and Milton Steinbach Fund, and Alcon Research Institute. The authors thank Elaine E. Smilko, Elizabeth A. M. Windsor, Andy Cheung, Mark Ayzenberg, and Michelle Doobrajh for their critical help with this work.

REFERENCES

1. Feeney L. Lipofuscin and melanin of human retinal pigment epithelium. Fluorescence, enzyme cytochemical, and ultrastructural studies. Invest. Ophthalmol. Visual Sci 1978;17:583–600. [PubMed: 669890]
2. Eldred GE, Katz ML. Fluorophores of the human retinal pigment epithelium: separation and spectral characterization. Exp. Eye Res 1988;47:71–86. [PubMed: 3409988]
3. Eldred GE, Lasky MR. Retinal age pigments generated by self-assembling lysosomotropic detergents. Nature 1993;361:724–726. [PubMed: 8441466]
4. Sparrow JR, Boulton M. RPE lipofuscin and its role in retinal pathobiology. Exp. Eye Res 2005;80:595–606. [PubMed: 15862166]
5. Weng J, Mata NL, Azarian SM, Tzekov RT, Birch DG, Travis GH. Insights into the function of Rim protein in photoreceptors and etiology of Stargardt's disease from the phenotype in abcr knockout mice. Cell 1999;98:13–23. [PubMed: 10412977]
6. Radu RA, Mata NL, Nusinowitz S, Liu X, Sieving PA, Travis GH. Treatment with isotretinoin inhibits lipofuscin accumulation in a mouse model of recessive Stargardt's macular degeneration. Proc. Natl. Acad. Sci. U.S.A 2003;100:4742–4747. [PubMed: 12671074]
7. Boulton M, Rozanowska M, Rozanowski B, Wess T. The photoreactivity of ocular lipofuscin. Photochem. Photobiol. Sci 2004;3:759–764. [PubMed: 15295632]
8. Sieving PA, Chaudhry P, Kondo M, Provenzano M, Wu D, Carlson TJ, Bush RA, Thompson DA. Inhibition of the visual cycle *in vivo* by 13-*cis* retinoic acid protects from light damage and provides a mechanism for night blindness in isotretinoin therapy. Proc. Natl. Acad. Sci. U.S.A 2001;98:1835–1840. [PubMed: 11172037]
9. Golczak M, Kuksa V, Maeda T, Moise AR, Palczewski K. Positively charged retinoids are potent and selective inhibitors of the *trans-cis* isomerization in the retinoid (visual) cycle. Proc. Natl. Acad. Sci. U.S.A 2005;102:8162–8167. [PubMed: 15917330]

NIH-PA Author Manuscript

NIH-PA Author Manuscript

NIH-PA Author Manuscript

10. Maiti P, Kong J, Kim SR, Sparrow JR, Allikmets R, Rando RR. Small molecule RPE65 antagonists limit the visual cycle and prevent lipofuscin formation. Biochemistry 2006;45:852–860. [PubMed: 16411761]
11. Travis GH, Golczak M, Moise AR, Palczewski K. Diseases caused by defects in the visual cycle: retinoids as potential therapeutic agents. Annu. Rev. Pharmacol. Toxicol 2007;47:8.1–8.44.
12. Kitagawa K, Nishida S, Ogura Y. *In vivo* quantitation of autofluorescence in human retinal pigment epithelium. Ophthalmologica 1989;199:116–121. [PubMed: 2587019]
13. Delori FC. Spectrophotometer for noninvasive measurement of intrinsic fluorescence and reflectance of ocular fundus. Appl. Opt 1994;33:7439–7452.
14. von Ruckmann A, Fitzke FW, Bird AC. Distribution of fundus autofluorescence with a scanning laser ophthalmoscope. Br. J. Ophthamol 1995;79:407–412.
15. Delori FC, Dorey CK, Staurenghi G, Arend O, Goger DG, Weiter JJ. *In vivo* fluorescence of the ocular fundus exhibits retinal pigment epithelium lipofuscin characteristics. Invest. Ophthalmol. Visual Sci 1995;36:718–729. [PubMed: 7890502]
16. Delori FC, Staurenghi G, Arend O, Dorey CK, Goger DG, Weiter JJ. *In vivo* measurement of lipofuscin in Stargardt's disease—fundus flavimaculatus. Invest. Ophthalmol. Visual Sci 1995;36:2327–2331. [PubMed: 7558729]
17. Bellmann C, Holz FG, Schapp O, Volcker HE, Otto TP. [Topography of fundus autofluorescence with a new confocal scanning laser ophthalmoscope]. Ophthalmologe 1997;94:385–391. [PubMed: 9312311](in German)
18. Holz FG, Bellmann C, Margaritidis M, Schutt F, Otto TP, Volcker HE. Patterns of increased *in vivo* fundus autofluorescence in the junctional zone of geographic atrophy of the retinal pigment epithelium associated with age-related macular degeneration. Graefe's Arch. Clin. Exp. Ophthalmol 1999;237:145–152. [PubMed: 9987631]
19. Delori FC, Goger DG, Dorey CK. Age-related accumulation and spatial distribution of lipofuscin in RPE of normal subjects. Invest. Ophthalmol. Visual Sci 2001;42:1855–1866. [PubMed: 11431454]
20. Holz FG, Bellman C, Staudt S, Schutt F, Volcker HE. Fundus autofluorescence and development of geographic atrophy in age-related macular degeneration. Invest. Ophthalmol. Visual Sci 2001;42:1051–1056. [PubMed: 11274085]
21. Lois N, Holder GE, Bunce C, Fitzke FW, Bird AC. Phenotypic subtypes of Stargardt macular dystrophy—fundus flavimaculatus. Arch. Ophthalmol 2001;119:359–369. [PubMed: 11231769] (Chicago)
22. Gerth C, Andrassi-Darida M, Bock M, Preising MN, Weber BH, Lorenz B. Phenotypes of 16 Stargardt macular dystrophy/fundus flavimaculatus patients with known *ABCA*4 mutations and evaluation of genotype-phenotype correlation. Graefes Arch. Clin. Exp. Ophthalmol 2002;240:628–638. [PubMed: 12192456]
23. Spaide RF. Fundus autofluorescence and age-related macular degeneration. Ophthalmology 2003;110:392–329. [PubMed: 12578786]
24. Lois N, Halfyard AS, Bird AC, Holder GE, Fitzke FW. Fundus autofluorescence in Stargardt macular dystrophy—fundus flavimaculatus. Am. J. Ophthalmol 2004;138:55–63. [PubMed: 15234282]
25. Jorzik JJ, Bindewald A, Dithmar S, Holz FG. Digital simultaneous fluorescein and indocyanine green angiography, autofluorescence, and red-free imaging with a solid-state laser-based confocal scanning laser ophthalmoscope. Retina 2005;25:405–416. [PubMed: 15933585]
26. Schmitz-Valckenberg S, Bindewald-Wittich A, Dolar-Szczasny J, Dreyhaupt J, Wolf S, Scholl HP, Holz FG, Fundus Autofluorescence in Age-Related Macular Degeneration Study Group. Correlation between the area of increased autofluorescence surrounding geographic atrophy and disease progression in patients with AMD. Invest. Ophthalmol. Visual Sci 2006;47:2648–2654. [PubMed: 16723482]
27. Hwang JC, Chan JW, Chang S, Smith RT. Predictive value of fundus autofluorescence for development of geographic atrophy in age-related macular degeneration. Invest. Ophthalmol. Visual Sci 2006;47:2655–2661. [PubMed: 16723483]
28. Sunness JS, Ziegler MD, Applegate CA. Issues in quantifying atrophic macular disease using retinal autofluorescence. Retina 2006;26:666–672. [PubMed: 16829810]

NIH-PA Author Manuscript

NIH-PA Author Manuscript

NIH-PA Author Manuscript

29. Fishman GA, Jacobson SG, Alexander KR, Cideciyan AV, Birch DG, Weleber RG, Hood DC. Outcome measures and their application in clinical trials for retinal degenerative disease: outline, review, and perspective. Retina 2005;25:772–777. [PubMed: 16141867]
30. Delori FC, Parker JS, Mainster MA. Light levels in fundus photography and fluorescein angiography. Vision Res 1980;20:1099–1104. [PubMed: 7269267]
31. Piccolino FC, Borgia L, Zinicola E, Iester M, Torrielli S. Pre-injection fluorescence in indocyanine green angiography. Ophthalmology 1996;103:1837–1845. [PubMed: 8942879]
32. Weinberger AW, Lappas A, Kirschkamp T, Mazinani BA, Huth JK, Mohammadi B, Walter P. Fundus near infrared fluorescence correlates with fundus near infrared reflectance. Invest. Ophthalmol. Visual Sci 2006;47:3098–3108. [PubMed: 16799056]
33. Keilhauer CN, Delori FC. Near-infrared autofluorescence imaging of the fundus: visualization of ocular melanin. Invest. Ophthalmol. Visual Sci 2006;47:3556–3564. [PubMed: 16877429]
34. Cideciyan AV, Aleman TS, Swider M, Schwartz SB, Steinberg JD, Brucker AJ, Maguire AM, Bennett J, Stone EM, Jacobson SG. Mutations in *ABCA*4 result in accumulation of lipofuscin before slowing of the retinoid cycle: a reappraisal of the human disease sequence. Hum. Mol. Genet 2004;13:525–534. [PubMed: 14709597]
35. Cideciyan AV, Swider M, Aleman TS, Sumaroka A, Schwartz SB, Roman MI, Milam AH, Bennett J, Stone EM, Jacobson SG. *ABCA*4-associated retinal degenerations spare structure and function of the human parapapillary retina. Invest. Ophthalmol. Visual Sci 2005;46:4739–4746. [PubMed: 16303974]
36. Cideciyan AV, Jacobson SG, Aleman TS, Gu D, Pearce-Kelling SE, Sumaroka A, Acland GM, Aguirre GD. *In vivo* dynamics of retinal injury and repair in the rhodopsin mutant dog model of human retinitis pigmentosa. Proc. Natl. Acad. Sci. U.S.A 2005;102:5233–5238. [PubMed: 15784735]
37. Galloway MM. Texture analysis using gray level run-lengths. Comput. Graph. Image Process 1975;4:172–179.
38. Herlidou S, Grebe R, Grados F, Leuyer N, Fardellone P, Meyer ME. Influence of age and osteoporosis on calcaneus trabecular bone structure: a preliminary *in vivo* MRI study by quantitative texture analysis. Magn. Reson. Imaging 2004;22:237–243. [PubMed: 15010116]
39. Jacobson SG, Aleman TS, Cideciyan AV, Sumaroka A, Schwartz SB, Windsor EAM, Traboulsi EI, Heon E, Pittler SJ, Milam AH, Maguire AM, Palczewski K, Stone EM, Bennett J. Identifying photoreceptors in blind eyes due to RPE65 mutations: prerequisite for human gene therapy success. Proc. Natl. Acad. Sci. U.S.A 2005;102:6177–6182. [PubMed: 15837919]
40. Jacobson SG, Cideciyan AV, Sumaroka A, Aleman TS, Schwartz SB, Windsor EAM, Roman AJ, Stone EM, MacDonald IM. Remodeling of the human retina in choroideremia—Rab Escort Protein 1 (REP-1) mutations. Invest. Ophthalmol. Visual Sci 2006;47:4113–4120. [PubMed: 16936131]
41. Huang Y, Cideciyan AV, Papastergiou GI, Banin E, Semple-Rowland SL, Milam AH, Jacobson SG. Relation of optical coherence tomography to microanatomy in normal and *rd* chickens. Invest. Ophthalmol. Visual Sci 1998;39:2405–2416. [PubMed: 9804149]
42. Elsner AE, Burns SA, Weiter JJ, Delori FC. Infrared imaging of sub-retinal structures in the human ocular fundus. Vision Res 1996;36:191–205. [PubMed: 8746253]
43. Delori FC, Goger DG, Keilhauer C, Salvetti P, Staurenghi G. Bimodal spatial distribution of macular pigment: evidence of a gender relationship. J. Opt. Soc. Am. A 2006;23:521–538.
44. Knighton RW, Jacobson SG, Kemp CM. The spectral reflectance of the nerve fiber layer of the macaque retina. Invest. Ophthalmol. Visual Sci 1989;30:2392–2402. [PubMed: 2807795]
45. Allikmets R, Singh N, Sun H, Shroyer NF, Hutchinson A, Chidambaram A, Gerrard B, Baird L, Stauffer D, Peiffer A, Rattner A, Smallwood P, Li Y, Anderson KL, Lewis RA, Nathans J, Leppert M, Dean M, Lupski JR. A photoreceptor cell-specific ATP-binding transporter gene (*ABCR*) is mutated in recessive Stargardt macular dystrophy. Nat. Genet 1997;15:236–246. [PubMed: 9054934]
46. Martinez-Mir A, Paloma E, Allikmets R, Ayuso C, del Rio T, Dean M, Vilageliu L, Gonzalez-Duarte R, Balcells S. Retinitis pigmentosa caused by a homozygous mutation in the Stargardt disease gene *ABCR*. Nat. Genet 1998;18:11–12. [PubMed: 9425888]
47. Cremers FP, van de Pol DJ, van Driel M, den Hollander AI, van Haren FJ, Knoers NV, Tijmes N, Bergen AA, Rohrschneider K, Blankenagel A, Pinckers AJ, Deutman AF, Hoyng CB. Autosomal

NIH-PA Author Manuscript

NIH-PA Author Manuscript

NIH-PA Author Manuscript

recessive retinitis pigmentosa and cone-rod dystrophy caused by splice site mutations in the Stargardt's disease gene *ABCR*. Hum. Mol. Genet 1998;7:355–362. [PubMed: 9466990]

48. Fishman GA, Stone EM, Grover S, Derlacki DJ, Haines HL, Hockey RR. Variation of clinical expression in patients with Stargardt dystrophy and sequence variations in the *ABCR* gene. Arch. Ophthalmol 1999;117:504–510. [PubMed: 10206579](Chicago)
49. Webster AR, Heon E, Lotery AJ, Vandenburgh K, Casavant TL, Oh KT, Beck G, Fishman GA, Lam BL, Levin A, Heckenlively JR, Jacobson SG, Weleber RG, Sheffield VC, Stone EM. An analysis of allelic variation in the *ABCA*4 gene. Invest. Ophthalmol. Visual Sci 2001;42:1179–1189. [PubMed: 11328725]
50. Fishman GA, Stone EM, Eliason DA, Taylor CM, Lindeman M, Derlacki DJ. *ABCA*4 gene sequence variations in patients with autosomal recessive cone-rod dystrophy. Arch. Ophthalmol 2003;121:851–855. [PubMed: 12796258](Chicago)
51. Aleman TS, Cideciyan AV, Windsor EAM, Schwartz SB, Gardner LM, Emmons JM, Duncan KG, Steinberg JD, Stone EM, Jacobson SG. Macular pigment in *ABCA*4-associated retinal degenerations: response to lutein supplementation. Invest. Ophthalmol. Visual Sci 2006;47E-Abstract 5810
52. Hopkins J, Walsh A, Chakravarthy U. Fundus autofluorescence in age-related macular degeneration: an epiphenomenon? Invest. Ophthalmol. Visual Sci 2006;47:2269–2271. [PubMed: 16723433]
53. Sliney D, Aron-Rosa D, Delori F, Fankhauser F, Landry R, Mainster M, Marshall J, Rassow B, Stuck B, Trokel S, West TM, Wolffe M, International Commission on Non-Ionizing Radiation Protection. Adjustment of guidelines for exposure of the eye to optical radiation from ocular instruments: statement from a task group of the International Commission on Non-Ionizing Radiation Protection (ICNIRP). Appl. Opt 2005;44:2162–2176. [PubMed: 15835362]
54. Paskowitz DM, Lavail MM, Duncan JL. Light and inherited retinal degeneration. Br. J. Ophthamol 2006;90:1060–1066.
55. Schraermeyer U. Does melanin turnover occur in the eyes of adult vertebrates? Pigment Cell Res 1993;6:193–204. [PubMed: 8248016]
56. Weiter JJ, Delori FC, Wing GL, Fitch KA. Retinal pigment epithelial lipofuscin and melanin and choroidal melanin in human eyes. Invest. Ophthalmol. Visual Sci 1986;27:145–152. [PubMed: 3943941]
57. Gibbs D, Azarian SM, Lillo C, Kitamoto J, Klomp AE, Steel KP, Libby RT, Williams DS. Role of myosin VIIa and Rab27a in the motility and localization of RPE melanosomes. J. Cell. Sci 2004;117:6473–6483. [PubMed: 15572405]
58. Kayatz P, Thumann G, Luther TT, Jordan JF, Bartz-Schmidt KU, Esser PJ, Schraermeyer U. Oxidation causes melanin fluorescence. Invest. Ophthalmol. Visual Sci 2001;42:241–246. [PubMed: 11133875]
59. Tucker GS. Refractile bodies in the inner segments of cones in the aging human retina. Invest. Ophthalmol. Visual Sci 1986;27:708–715. [PubMed: 3009350]
60. Iwasaki M, Inomata H. Lipofuscin granules in human photoreceptor cells. Invest. Ophthalmol. Visual Sci 1988;29:671–679. [PubMed: 3366562]
61. Birnbach CD, Jarvelainen M, Possin DE, Milam AH. Histopathology and immunocytochemistry of the neurosensory retina in fundus flavimaculatus. Ophthalmology 1994;101:1211–1219. [PubMed: 8035984]
62. Fishkin N, Jang YP, Itagaki Y, Sparrow JR, Nakanishi K. A2-rhodopsin: a new fluorophore isolated from photoreceptor outer segments. Org. Biomol. Chem 2003;1:1101–1105. [PubMed: 12926382]

NIH-PA Author Manuscript
NIH-PA Author Manuscript
NIH-PA Author Manuscript

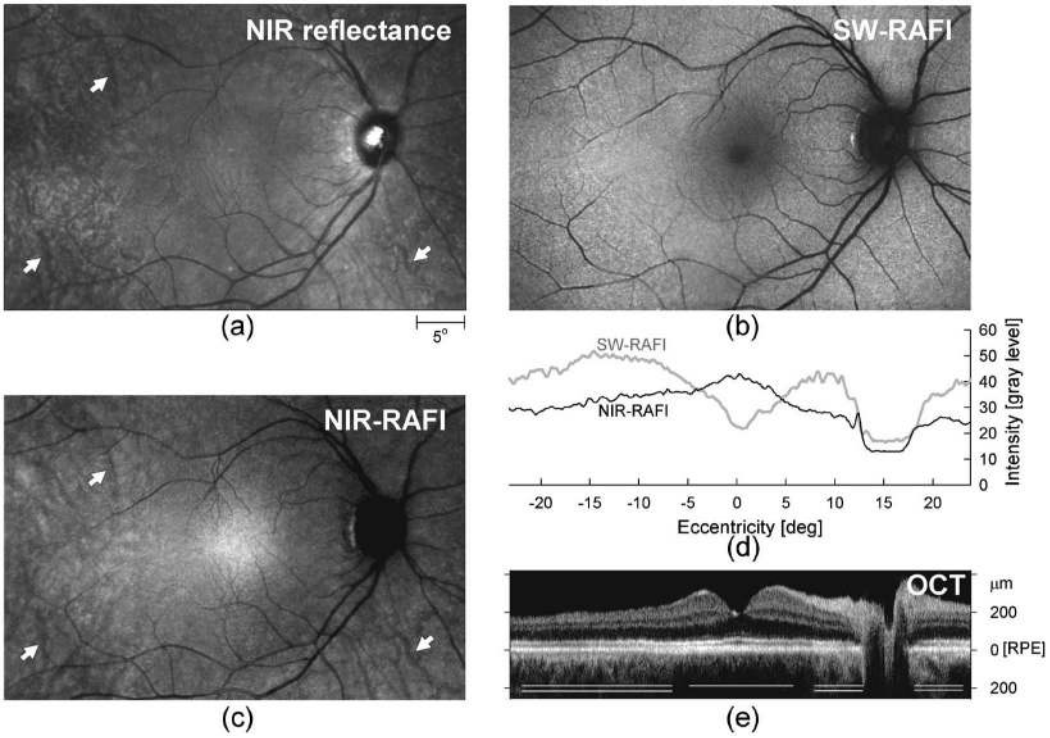

Fig. 1.

Illustration of different imaging modalities in a 43-year-old representative normal subject NIR-reflectance (a), SW-RAFI (b), and NIR-RAFI (c) mosaics of the central retina are shown spatially registered with respect to one another. Choroidal vasculature is apparent in some retinal regions with NIR imaging (arrows). Images are individually contrast stretched for visibility of features, and thus intensity of pixels is not comparable between images. Actual recorded RAFI intensities are shown (d) in gray-level units for SW-RAFI (gray trace) and NIR-RAFI (black trace) modalities along the horizontal meridian. An extended OCT mosaic along the horizontal meridian is also shown (e) coregistered to the profiles and the images. Retinal depth of zero corresponds to the approximate location of the RPE. Central macular region (single line) shows less backscatter signal originating from sub-RPE layers compared with more peripheral regions (double lines) where NIR light appears to penetrate deeper.

NIH-PA Author Manuscript
NIH-PA Author Manuscript
NIH-PA Author Manuscript

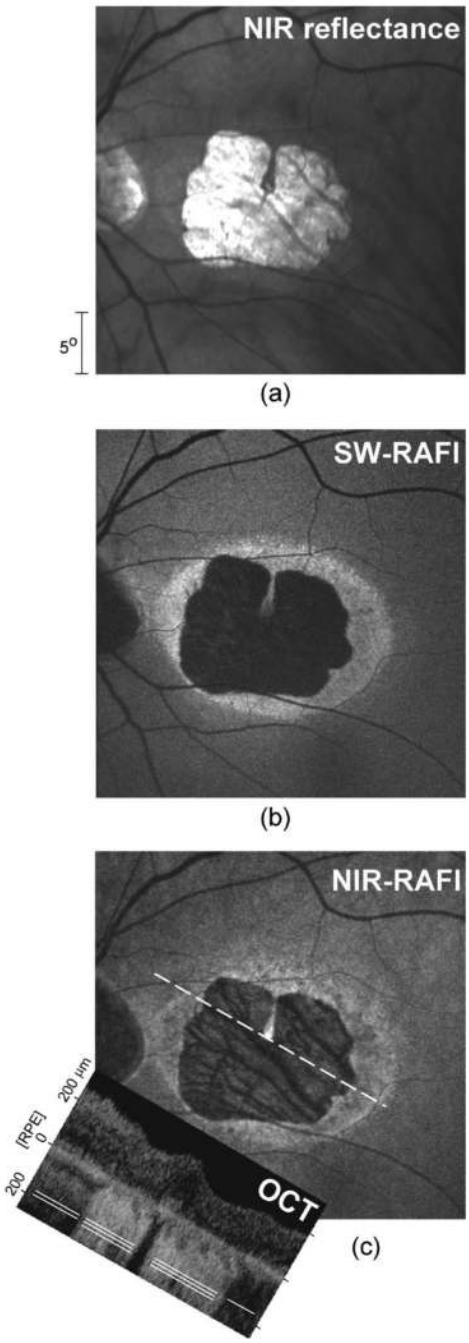

Fig. 2.

Interpretation of RAFI intensities in severe RPE disease in patient 7 (a) NIR-reflectance image showing a well-delineated macular lesion. The approximately two-fold greater reflectance within the lesion is likely due to depigmentation or atrophy of the RPE. (b) SW-RAFI of the central retina showing dramatically reduced lipofuscin autofluorescence within the lesion. Surrounding the lesion is an irregular annulus of hyperautofluorescence. (c) NIR-RAFI shows both similarities to and differences from SW-RAFI. Choroidal vessels are distinctly apparent within the lesion. Inset: OCT image obtained at an angle (dashed white line) through the fovea shows the transition from a high (triple lines) to a relatively low (single line) sub-RPE backscatter region at the temporal boundary of the lesion.

NIH-PA Author Manuscript
NIH-PA Author Manuscript
NIH-PA Author Manuscript

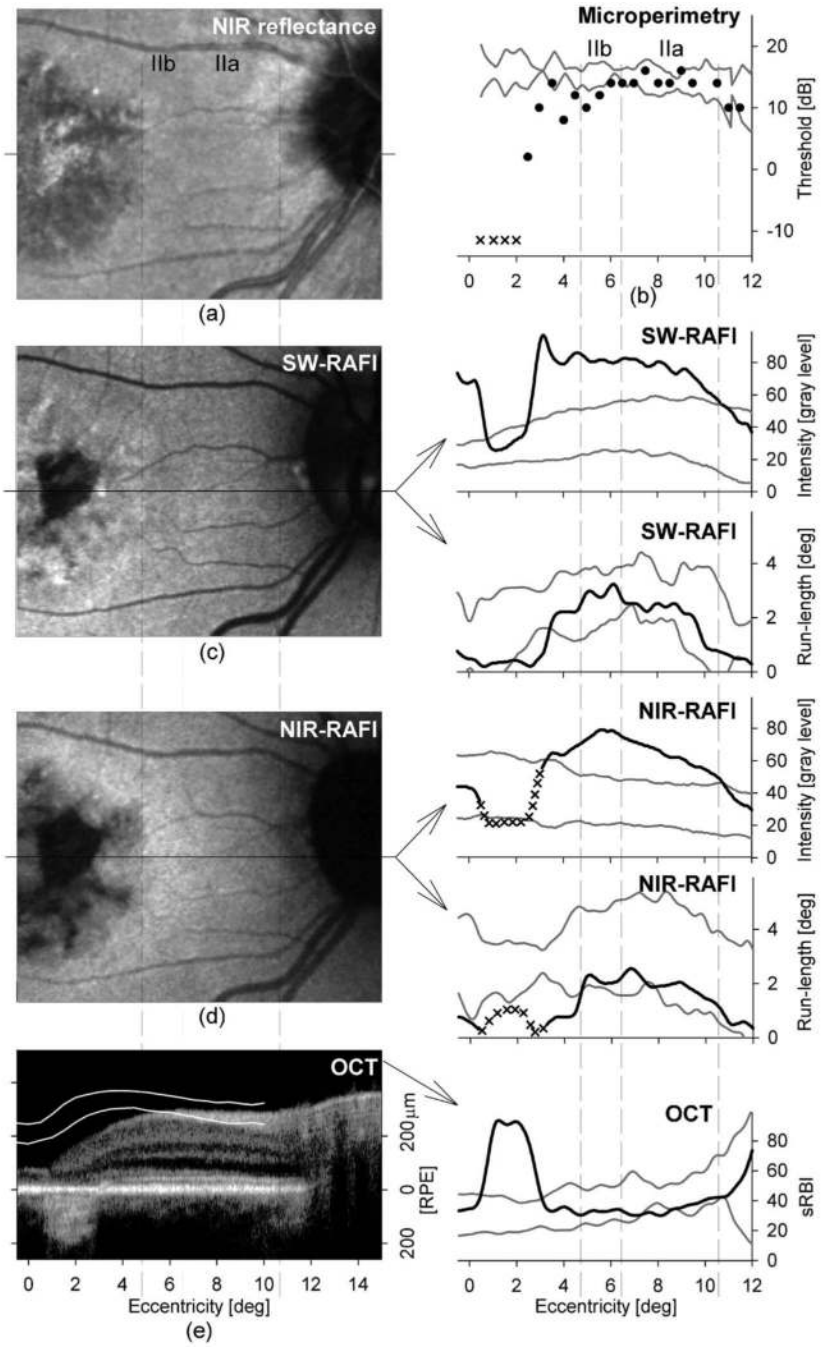

Fig. 3.

Qualitative and quantitative analyses of central disease between the fovea and the optic nerve head in a representative patient (patient 6) with early/mild *ABCA*4 disease (a) NIR-reflectance image showing the clinically overt maculopathy surrounded by normal appearing retina. (b) Microperimetry thresholds (in decibels, dB) with red-on-red stimulus. Stimuli not seen with red-on-red and white-on-red conditions are shown as x's at the equivalent red-on-red threshold of −12.5 dB. (c) SW-RAFI image showing a parafoveal region of severe RPE disease. Intensity and run-length values quantified along the horizontal profile are shown on the right panels. (d) NIR-RAFI image shows similarities to and differences from SW-RAFI. Intensity and run-length values quantified along the horizontal profile are shown on the right panels. Regions of

NIH-PA Author Manuscript

NIH-PA Author Manuscript

NIH-PA Author Manuscript

the retina with enrichment of choroidal component to the NIR-RAFI signal are marked as uninterpretable (x). All images (a,c,d) are shown individually contrast stretched for visibility of features. (e) OCT scan along the horizontal profile. Pair of overlaid white lines represents the normal limits of retinal thickness from the RPE peak (retinal depth of 0 μm). Estimated sub-RPE backscatter index (sRBI) is shown to the right. Boundaries of subclinical disease stages IIa and IIb are shown with vertical dashed lines coregistered in both columns across all panels. Pairs of gray lines on right panels represent normal limits (mean±2 SD) for each measure.

NIH-PA Author Manuscript
NIH-PA Author Manuscript
NIH-PA Author Manuscript

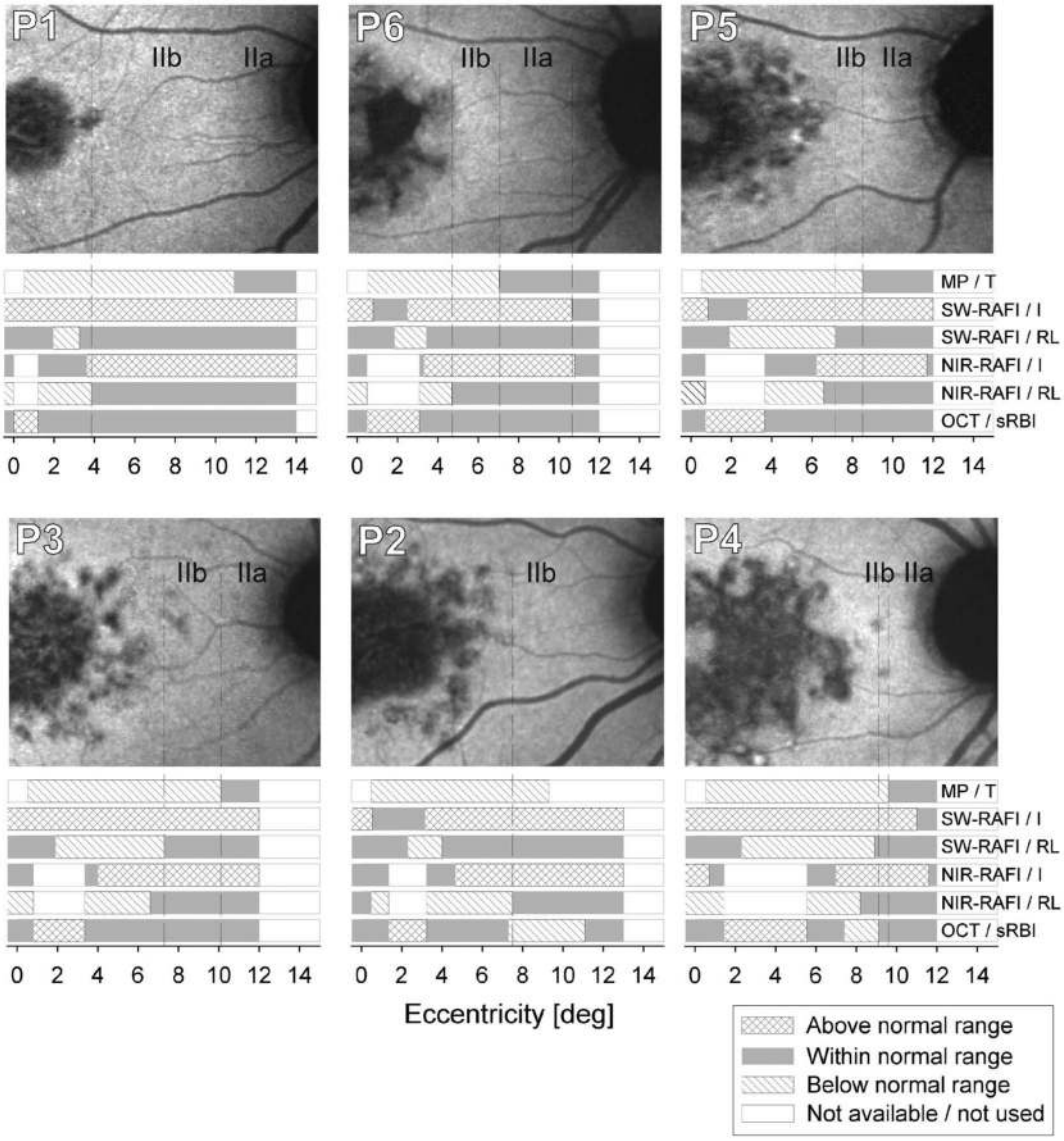

Fig. 4.

NIR-RAFI images and colocalized summary of all quantified parameters along the foveo-papillary profile in six patients All images are shown individually contrast stretched for visibility of features. The parameters include microperimetry thresholds (MP/T); SW-RAFI intensity (SW-RAFI/I) and run-length (SW-RAFI/RL); NIR-RAFI intensity (NIR-RAFI/I) and run-length (NIR-RAFI/RL); and OCT-based sub-RPE backscattering index (OCT/sRBI). Parameters at each retinal location are classified into "within normal range" (graybars), "above normal range" (cross-hatched bars), and "below normal range" (hatched bars). Retinal loci where data were not available or NIR-RAFI was excluded because of above-normal sRBI values are specified as "not available/not used" (white). Boundaries of subclinical stage IIa and IIb disease are shown on NIR-RAFI images with dashed lines extended from parameter results.

NIH-PA Author Manuscript NIH-PA Author Manuscript NIH-PA Author Manuscript

Table 1

Clinical and Molecular Characteristics of Patients

Patient Number	Age (yr)/Gender	*ABCA4* Mutation	Visual Acuity[c]		Refraction[d]	
			RE	LE	RE	LE
1	21/M	R152X/G1961E	20/100	20/100	+0.00	+0.25
2	25/F	R1129L/L1940P	20/100	20/100	−0.25	−0.75
3	30/M	T1019M/G1961E	20/100	20/100	−2.00	−2.00
4	32/F	V935A/IVS40+5G>A	20/30	20/40	−0.75	−1.25
5[a]	42/F	V256V/G1961E	20/30	20/20	−2.75	−2.75
6[a]	46/F	V256V/G1961E	20/32	20/40	−0.75	−1.00
7	53/M	[b]	20/20	20/25	−6.25	−9.00

[a] Patients are siblings.

[b] Mutation unknown; clinical diagnosis bilateral maculopathy.

[c] Best corrected visual acuity; RE, right eye; LE, left eye.

[d] Spherical equivalent. RE, right eye; LE, left eye.

J Opt Soc Am A Opt Image Sci Vis. Author manuscript; available in PMC 2008 November 5.